Check for updates

A highly sensitive photonic crystal fiber temperature sensor based on Sagnac interferometer with full liquid filling

Yinping Zhang[1] · **Xiuqing Zhang**[1] · **Shichao Chu**[1] · **Zhenkai Fan**[1]

Abstract

A highly sensitive photonic crystal fiber temperature sensor based on Sagnac interferometer with full liquid filling is proposed. All of the air holes in the PCF are filled with temperature-sensitive liquid, the structure is analyzed theoretically and numerically using the finite element method. Since the sensitivity is related to the group birefringent grating, the size of the sensitivity can be reflected by comparing the absolute value of the group birefringent grating. The structure is optimized by modifying the diameter of d_0, d_1 and d_2 of the air holes for the photonic crystal fiber. In the process of numerical calculation, the best parameters are selected by comparing the absolute value of the group birefringent grating near the special wavelength to obtain higher sensitivity. The average sensitivity of 35.14 nm/°C and -27.71 nm/°C are obtained at 27–32 °C in a parametrically optimized structure and R^2 are 0.98455 and 0.9779. The RI sensitivity is also studied as RI changes from 1.404 to 1.409, the average sensitivity are $-53{,}714$ nm/RIU and $-47{,}714.29$ nm/RIU.

1 Introduction

Photonic crystal fibers (PCFs), also known as microstructured fibers or porous fibers, are a new type of conductive fiber media. The emergence of the internet has promoted the high standard requirements in the field of communication with the continuous update and development of science and technology, such as large capacity, high efficiency, low cost and so on, which are the goals people are striving to pursue. Fiber optic electronic devices are also developing rapidly in this field. The performance of PCF can be changed by filling different materials in the air holes of the fiber, such as

✉ Xiuqing Zhang
  zhangxiuqing@hebust.edu.cn

✉ Zhenkai Fan
  zhkfan@hebust.edu.cn

1 School of Information Science and Engineering, Hebei University of Science and Technology, Shijiazhuang 050018, China

hydrogen (Couny et al. 2007), metals (Jiang et al. 2015), chloroform (Yang et al. 2013), ethanol (Wu et al. 2014), or temperature sensitive materials (Abramov et al. 1999). In recent years, the technology of combining optical fiber with sensing has become more mature, and optical fiber sensors have become research highlights. Scientists have conducted a lot of subject study on sagnac interferometer sensors to develop sensors in various application fields, such as temperature sensors (Zhang and Kahrizi 2007; Hirayama and Sano 2000; Fan et al. 2022), strain sensors (Qi et al. 2021), torsion sensors (Zhang et al. 2022), biochemical sensors (Mahajan et al. 2015) and so on.

The research of optical fiber temperature sensor based on sagnac interferometer has made rapid progress in continuous updating and development. In 2012, Zhao et al. (2012) studied a temperature sensor based on fiber sagnac interferometer (OFSI) and alcohol non-fully-filled high-birefringence photonic crystal fiber (HiBi-PCF). The temperature sensitivity of the sensor is approximately −1.17 nm/°C, which is only one-sixth of the fully filled HiBi-PCF OSFI. In 2015, Shao et al. (2015) designed a novel optical fiber temperature sensor using two cascaded sagnac interferometers, the sensitivity raised about 9 times. The data indicate that the sensitivity increases from 1.46 to 13.36 nm/°C. In 2016, Shi et al. (2016) proposed a temperature sensor based on a reflective sagnac fiber ring laser. The high temperature sensitivity is provided by downloading the reflective sagnac ring from the fiber-in-fiber ring laser as the filter and sensing head. A temperature sensor system with a temperature sensitivity of 1.739 nm/°C was obtained. In 2018, Shi et al. (2018) studied a high-sensitivity PCF temperature sensor based on sagnac interferometer. The temperature sensitivity were −8.7657 nm/°C and 16.8142 nm/°C when the temperature increases from 45 to 75 °C. The sensitivity were −7.848 nm/°C and 16.655 nm/°C when the temperature changes between 10 and 45 °C.

However, the optical fiber sensor based on sagnac interferometer with a single structure has been unable to meet people's requirement for measurement under different conditions. In 2019, Ma et al. (2019) devised a temperature sensor based on sagnac interferometer and liquid crystal PCF. The simulation results reveal that the temperature sensitivity and resolution can reach 15 nm/k and 6.7E−4 k in the range of 290–320 k. In 2020, Liu (2020) et al. invented a ring-shaped PCF temperature sensor based on sagnac interferometer (SI). During numerical analysis, one method is to fill the whole pore with temperature-sensitive liquid, which can realize single sensing interference inclination angle, and the average sensitivity reached 18.27 nm/°C. Another approach is to fill only large sized air holes with temperature sensitive liquid. And two sensing interference inclination angles with good linearity can be simultaneously realized. The corresponding mean sensitivities were 9.47 nm/°C and 8.57 nm/°C. In 2021, Md. Shakhawath Hossain et al. (2021) demonstrated a sulfide PCF temperature sensor based on sagnac interferometer. The simulation results display that the effect of the structure of total infiltration is better than the structure of local infiltration. The resulting sensitivities were −5.77 nm/°C and 8.49 nm/°C from 25 to 85 °C.

The proposed PCF temperature sensor based on sagnac interferometer, a full filling method was used to fill temperature sensitive liquid in the fiber cores of the PCF, and the parameters d_0, d_1 and d_2 that can affect the structural changes of the PCF are modified. The structure is selected by comparing the absolute values of the group birefringence grating near the special wavelength, the transmission spectrum of structures with different parameters are simulated. The average sensitivity can reach to 35.14 nm/°C and −27.71 nm/°C at 27–32°C, and R^2 are 0.98455 and 0.9779.

2 Geometry and theory

The cross section of the PCF structure proposed in this paper is shown in Fig. 1a. Six corners of the second cladding layer are removed to form the structure, and the air holes spacing Λ is 3.5 µm. d, d_0,d_1,d_2 represent the diameter of the air holes, the diameter of the air hole d = 2.8 µm. The diameter of the air hole d_1 was set larger to improve the birefringence of the PCF. The parameters d_0, d_1 and d_2 were changed in this paper. The background material of the PCF is fused silica, and its dispersion coefficient can be calculated by Sellmeier equation (Ghosh et al. 1994):

$$n^2(\lambda, T) = \left(1.31552 + 6.90754 \times 10^{-6}T\right) + \frac{\left(0.788404 + 23.5835 \times 10^{-6}T\right)\lambda^2}{\lambda^2 - \left(0.0110199 + 0.584758 \times 10^{-6}T\right)}$$
$$+ \frac{\left(0.91316 + 0.548368 \times 10^{-6}T\right)\lambda^2}{\lambda^2 - 100}$$

(1)

where the units of wavelength are microns and the units of temperature are degrees Celsius. All the air holes are filled with temperature sensitive liquid, which the refractive index is 1.37 when the temperature is 25 °C, and the sensitivity coefficient is −0.0004/°C (Liu et al. 2018). The relationship between refractive index and temperature can be expressed as n = 1.37–4×10^{-4}(T-25°C). The fabrication technology of PCFs has been very mature and achievable (He et al. 2021), so we believe that the structure assumed in this paper can be fabricated.

The fiber characteristics of the proposed structure are simulated and analyzed by finite element method. Similarly, we assume that it can reach the ideal state, set the scattering boundary conditions and perfect matching layer, and numerically calculate the dependence of refractive index and loss on the operable wavelength λ, as shown in Fig. 1b. The effective refractive index decreases with the wavelength increases, the limiting loss of optical fiber increases with wavelength increases. The lines and curves between the x and y polarization modes almost overlap each other.

The transmission spectrum of Sagnac interferometer can be obtained by the following formula (Han et al. 2013, 2014):
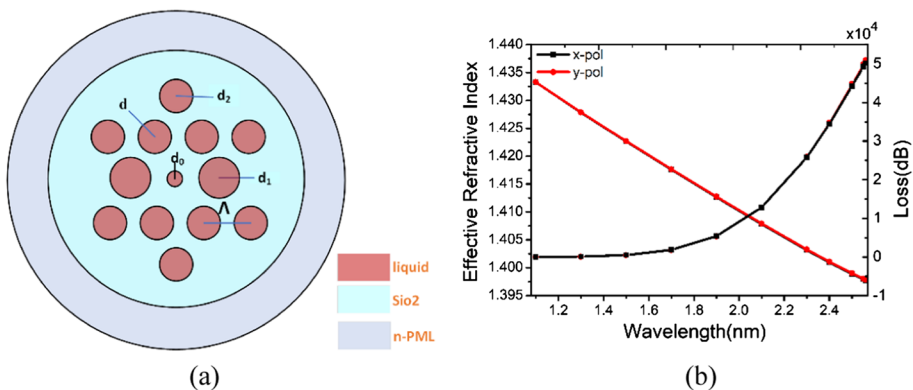
Fig. 1 **a** Schematic diagram of the cross-section of the PCF structure, **b** the effective refractive index and limiting loss dependence on the operational wavelength

$$T = \frac{1 - \cos(2\pi B(\lambda, T)L/\lambda)}{2} \quad (2)$$

where $2\pi B(\lambda, T)L/\lambda$ is the phase difference between x and y polarization mode. In the formula, B is a function of wavelength and temperature, representing phase birefringence, and its numerical expression is $B(\lambda, T) = n_x - n_y$, n_x, n_y indicates the refractive index of x and y polarization mode. L is the length of the PCF, λ is the resonant wavelength. When the phase matching condition is satisfied (namely, the following formula holds), λ will be obtained:

$$\frac{2\pi B(\lambda, T)L}{\lambda} = 2m\pi \quad (3)$$

where m is an integer. Taking the derivation of temperature T from both sides of the above equation, we can get:

$$\frac{\left[L\frac{\partial B(\lambda, T)}{\partial T} + L\frac{\partial B(\lambda, T)}{\partial \lambda}\frac{d\lambda(T)}{dT} + B(\lambda, T)\frac{dL}{dT}\right]\lambda(T) - B(\lambda, T)L\frac{d\lambda}{dT}}{\lambda^2(T)} = 0 \quad (4)$$

Then we can get the sensitivity dλ/dT:

$$S(T) = \frac{d\lambda}{dT} = \frac{\frac{\partial B(\lambda, T)}{\partial T}\lambda(T) + \frac{dL}{LdT}B(\lambda, T)\lambda(T)}{B_g(\lambda, T)} \quad (5)$$

where dL/L/dT is the temperature expansion coefficient of the filled liquid, which is ignored because it is very small. Group birefringence $B_g(\lambda, T) = B(\lambda, T) - \lambda dB(\lambda, T)/d\lambda$. According to the sensitivity formula, the highest sensitivity can be obtained near a specific wavelength when the denominator approaches zero. Therefore, we modify the structural parameters of d_0, d_1 and d_2 that can affect the group birefringence grating to conduct numerical simulation, compare the absolute value of the group birefringence B_g again, and finally optimize the structure to obtain the highest sensitivity.

3 Results and discussion

The schematic diagram of the temperature sensor system is shown in Fig. 2. The sensing system consists of six parts, including a broadband source (BBS), a spectrum analyzer (OSA), a 3db optical coupler (OC), a polarization controller (PC), a temperature chamber and a section of PCF designed by us. A beam of light is generated by BBS, and the light is divided into two beams through a 3db optical coupler. A beam of light transmits clockwise, first through the PC, and then through the PCF. The other beam of light is transmitted counterclockwise, first through PCF, and then through PC. The two beams of light are finally coupled together at the 3db optocoupler. The PCF is stored in a thermostatted chamber and has been tested for temperature sensitivity. The two beams of light produce a phase difference. The resulting interference fringes can be measured with OSA to detect temperature. The part marked with red in the Fig. 2 is the structure designed by us.

After the parameters were optimized for the designed structure, we obtained a high average sensitivity. The transmission spectrum is shown in Fig. 3a with structural parameters $d_0 = 0.6$ μm, $d_1 = 3.2$ μm, $d_2 = 3.1$ μm. The fiber length of the PCF is 26 cm, and the
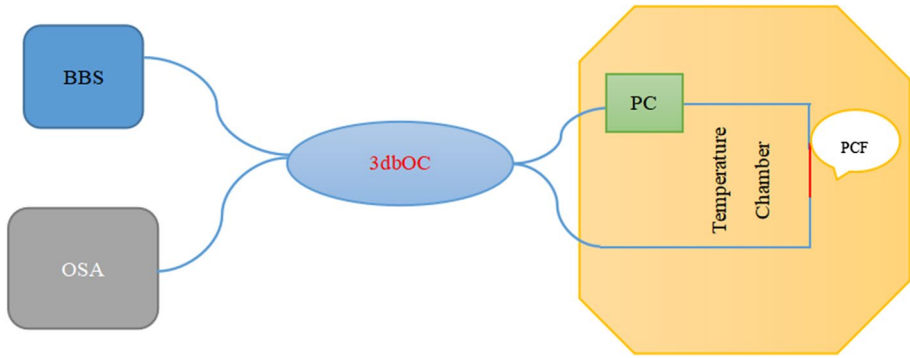
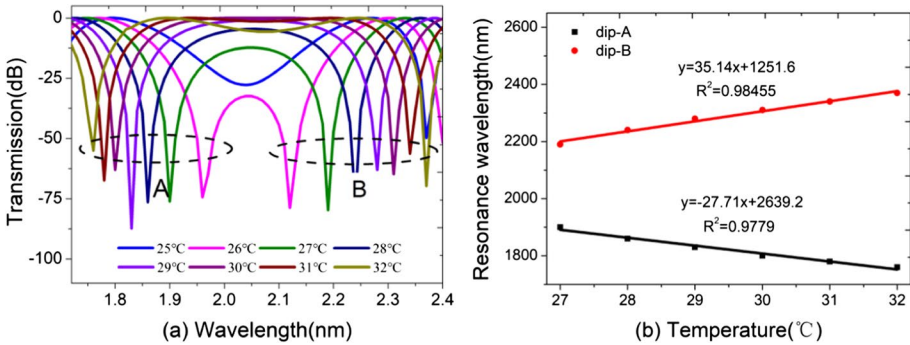**Fig. 2** Schematic diagram of temperature sensor system

Fig. 3 a The transmission spectrum dependence on the operable wavelength, **b** the resonance wavelength dependence on the temperature

temperature changes from 25 to 32 °C. Two dip wavelengths A and B appear in the range of 26–32 °C. The dip wavelength B shifts to long wavelength and the dip wavelength A shifts to short wavelength with the temperature increases. When the temperature is 25 °C, the dip wavelengths A and B become one dip wavelength, and when the temperature drops slightly, they are still one dip wavelength. The dip wavelengths A and B dependence on the temperature is shown in Fig. 3b. The dip wavelength B increases and the dip wavelength A decreases as the temperature increases. The obtained curve equations of dip wavelength A and dip wavelength B with temperature are $y = -0.27104x^3 + 25.83911x^2 - 844.32997x + 11,242.1904$, $y = 0.20202x^3 - 18.75541x^2 + 597.26768x - 3995.42857$. The average sensitivities are 35.14 nm/°C and -27.71 nm/°C when the temperatures are varied in the range from 27 to 32 °C, and R^2 are 0.98455 and 0.9779.

Figure 4 show the group birefringent grating dependence on the operable wavelength λ under different structure parameters of d_0, d_1, d_2 and different refractive index of the liqulid. Figure 4a shows the change of the group birefringent grating when $d_1 = 3.2$ μm and $d_2 = 2.8$ μm. Within the wavelength range of 1.0–2.4 μm, the group birefringence grating increases slowly at short wavelength and decreases rapidly at long wavelength with d_0 increases. The dashed line indicates that the value of the group birefringent grating is zero. Figure 4b shows the change of the group birefringence grating when $d_0 = 1.2$ μm
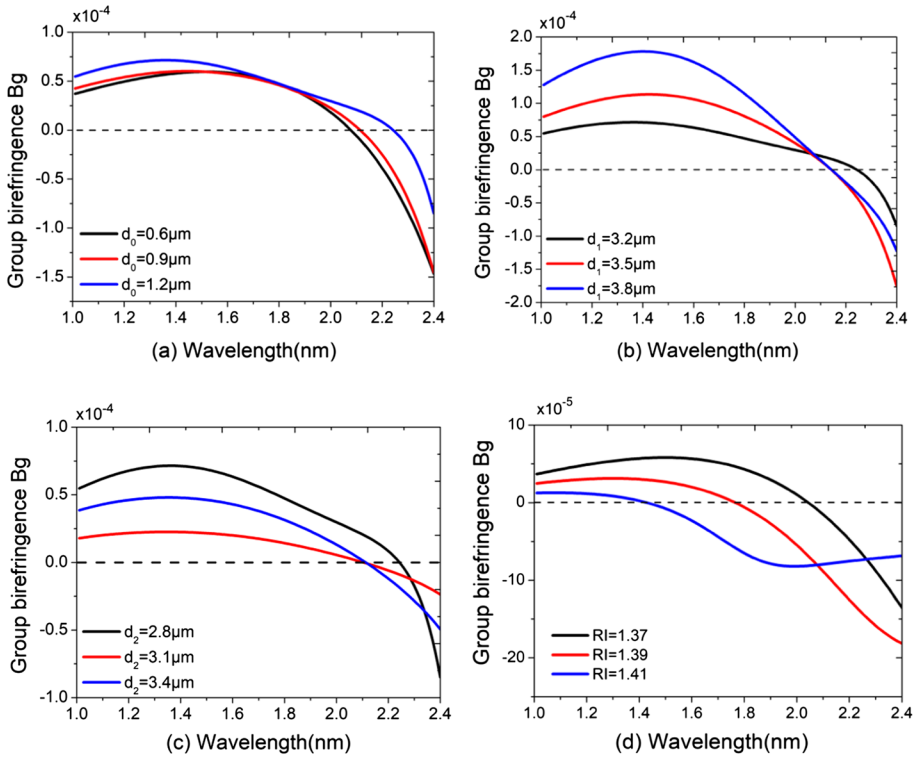
Fig. 4 The group birefringent grating dependence on the operable wavelength λ under different structure parameters of d_0, d_1, d_2 and different refractive index of the liqulid

and $d_2 = 2.8$ μm. The value of the zero point group birefringent grating increases before 1.4 μm and decreases rapidly with d_0 increases, the three lines have an intersection around 2.1 μm. Figure 4c shows the dependence of the group birefringent grating on the operable wavelength λ when $d_0 = 1.2$ μm and $d_1 = 3.2$ μm and d_2 changes from 2.8 to 3.4 μm. The group birefringent grating gradually increases first and then decreases with the diameter d_2 increases. Combined with the calculated data, we selected the final structural parameters are $d_0 = 0.6$ μm, $d_1 = 3.2$ μm and $d_2 = 3.1$ μm. Its transmission spectrum was calculated by finite element method, and then its sensitivity was analyzed.

Figure 4d shows the the group birefringent grating dependence on the operable wavelength λ under different refractive index of the liqulid, and the parameters are $d_0 = 0.6$ μm, $d_1 = 3.2$ μm and $d_2 = 3.1$ μm. When RI = 1.37 and 1.39, the group birefringence increases firstly and then decreases with the wavelength increases. When RI = 1.41, the value of group birefringence gradually decreases first and then increases slowly, and is the smallest absolute value among them. So we calculate the sensitivity of the refractive index near the RI of 1.4.

Figure 5 show the transmission spectrum dependence on the wavelength of the parameters within a certain range of the parameters (a) $d_0 = 0.6$ μm, $d_1 = 3.2$ μm, $d_2 = 2.8$ μm. (b) $d_0 = 1.2$ μm, $d_1 = 3.5$ μm, $d_2 = 2.8$ μm. (c) $d_0 = 1.2$ μm, $d_1 = 3.2$ μm, $d_2 = 3.1$ μm. (d) $d_0 = 1.2$ μm, $d_1 = 3.2$ μm, $d_2 = 2.8$ μm, respectively. As the wavelength increases, the transmission spectrum shows a periodic change. The wavelength range shown in the figure is
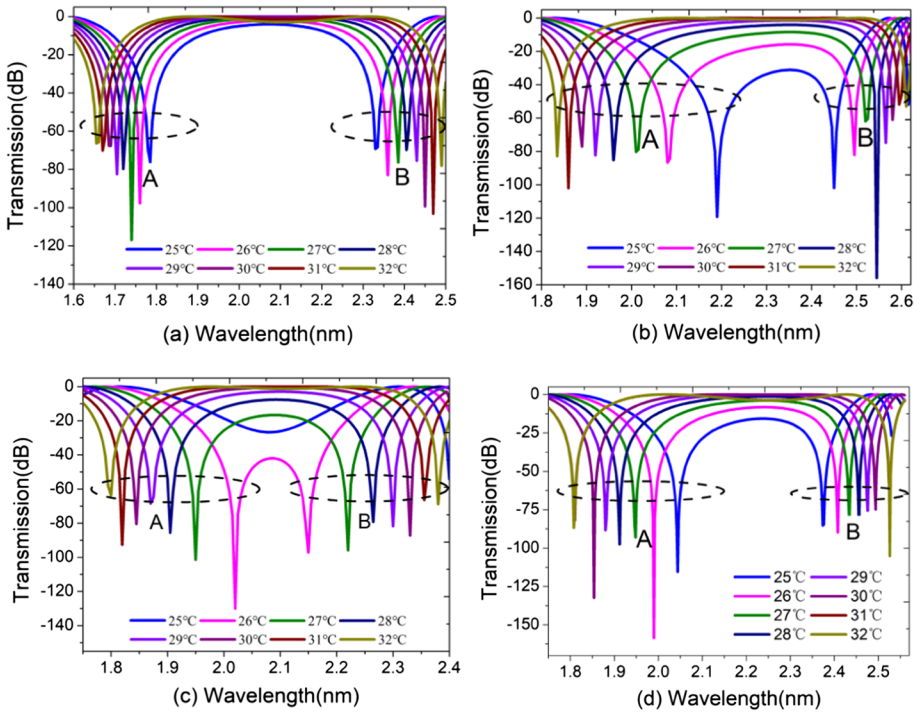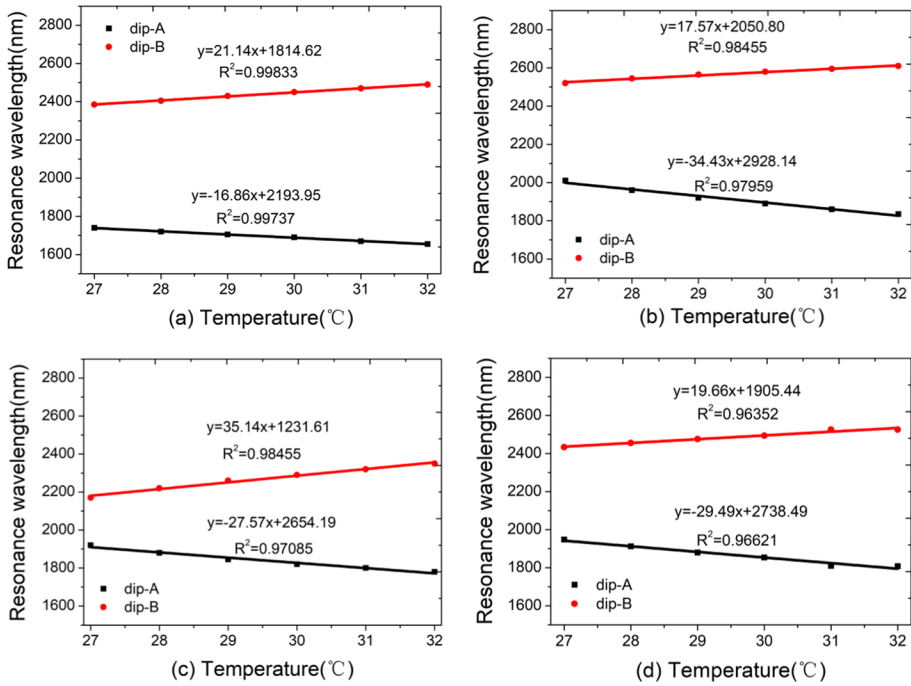
Fig. 5 The transmission spectrum dependence on the wavelength of the parameters **a** $d_0=0.6$ µm, $d_1=3.2$ µm, $d_2=2.8$ µm, **b** $d_0=1.2$ µm, $d_1=3.5$ µm, $d_2=2.8$ µm, **c** $d_0=1.2$ µm, $d_1=3.2$ µm, $d_2=3.1$ µm, **d** $d_0=1.2$ µm, $d_1=3.2$ µm, $d_2=2.8$ µm, respectively
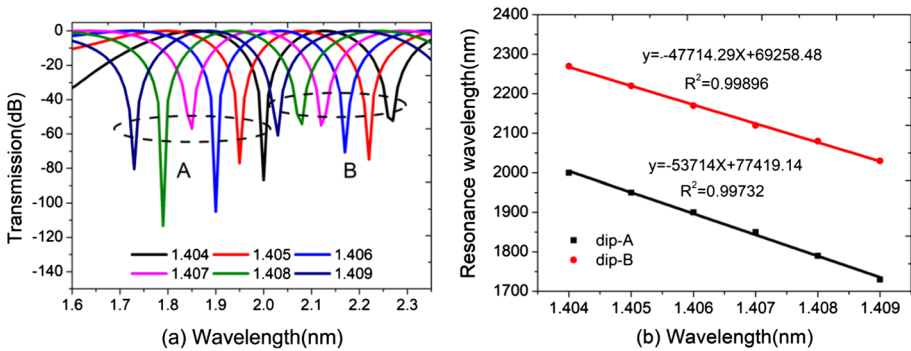
selected to better show the dependence of the transmission spectrum on the wavelength. In Fig. 5, the movement directions of the dip wavelength A and the dip wavelength B are opposite. The dip wavelength A moves to the short wavelength direction, and the dip wavelength B moves to the long wavelength direction. Figure 5a shows that wavelength range shift by the two dip wavelength is minimal, Fig. 5b shows that the wavelength range shift by the dip wavelength A is greater than the wavelength range shifted by the dip wavelength B. In Fig. 5c, d, the wavelength ranges of the two dip wavelength shift similarly, and it can be seen that the shift of the wavelength range of dip wavelength A is greater than that of dip wavelength B.

Figure 6 correspond to the fitting resonance wavelength dependence on the temperature of the parameters (a) $d_0=0.6$ µm, $d_1=3.2$ µm, $d_2=2.8$ µm. (b) $d_0=1.2$ µm, $d_1=3.5$ µm, $d_2=2.8$ µm. (c) $d_0=1.2$ µm, $d_1=3.2$ µm, $d_2=3.1$ µm. (d) $d_0=1.2$ µm, $d_1=3.2$ µm, $d_2=2.8$ µm, respectively. The slope of the curves represent the average sensitivity of 27–32 °C. The sensitivities of the dip wavelength A and the dip wavelength B are -16.86 nm/°C, 21.14 nm/°C, -34.43 nm/°C, 17.57 nm/°C, -27.57 nm/°C, 35.14 nm/°C, -29.49 nm/°C and 19.66 nm/°C, respectively.

Figure 7a shows the transmission spectrum dependence on the operable wavelength when the refractive index is 1.404–1.409, and the structural parameters are $d_0=0.6$ µm, $d_1=3.2$ µm and $d_2=3.1$ µm. When the refractive index increases, the dip wavelength A and the dip wavelength B moves to the short wavelength direction. Figure 7b shows the

Fig. 6 The resonance wavelength dependence on the operational wavelength under different parameters **a** $d_0 = 0.6$ μm, $d_1 = 3.2$ μm, $d_2 = 2.8$ μm, **b** $d_0 = 1.2$ μm, $d_1 = 3.5$ μm, $d_2 = 2.8$ μm, **c** $d_0 = 1.2$ μm, $d_1 = 3.2$ μm, $d_2 = 3.1$ μm, **d** $d_0 = 1.2$ μm, $d_1 = 3.2$ μm, $d_2 = 2.8$ μm, respectively

Fig. 7 a The transmission spectrum dependence on the operable wavelength, **b** the resonance wavelength dependence on the effective refractive index

resonance wavelength dependence on the effective refractive index. The average sensitivities are $-53,714$ nm/RIU and $-47,714.29$ nm/RIU, and R^2 are 0.99732 and 0.99896.

As shown in Table 1, in the literature we investigated, the sensitivity of the interferometric sensor was higher than that of the surface plasmon resonance sensor, and the sensitivity obtained over a wide measurement range was much lower than that of ours. The sensitivity of the sagnac interferometric sensor was slightly higher than that of other interferometric sensors.

Table 1 Performance comparison of the PCF temperature sensor

Senser type	Detecting window (°C)	Sensitivity(nm/°C)	Reference
Surface plasmon resonance	0–45	0.3769	Ibrahim et al. (2019)
Fabry–Perot	20–80	− 1.20507	Liu et al. (2022)
Mach–Zehnder	30–80	− 0.3056	Ma et al. (2022)
Sagnac	− 25–85	1.5005	Zhao et al. (2020)
Our structure	25–32	35.14, − 27.71	

Compared with other sensors, it is our advantage to obtain high sensitivity in a small range. Our structure is simple and easy to realize, with high sensitivity and precision. And it is expect to be reused in the field of temperature and refractive index measurement.

4 Conclusion

In this paper, a high-sensitivity PCF temperature sensor based on sagnac interferometer full liquid filling is presented. All the air holes of the PCF are filled with temperature-sensitive liquid, and the designed fiber structure is simple and easy to realize. We optimized the parameters d_0, d_1 and d_2 that can affect the group birefringent grating of the structure of the PCF. The optimal structure was selected by comparing the absolute value of the group birefringent grating at a range of wavelength. We plotted the transmission spectra of other structures with adjusted parameters and calculated the sensitivity. In the structure parameters are $d_0 = 0.6$ μm, $d_1 = 3.2$ μm and $d_2 = 3.1$ μm. The average sensitivity of 35.14 nm/°C and − 27.71 nm/°C are obtained at 27–32 °C, and R^2 are 0.98455 and 0.9779. The sensitivity of the refractive index of the liquid are − 53,714 nm/RIU and − 47,714 nm/RIU at RI ranging from 1.404 to 1.409.

Data availability Not applicable.

Declarations

Conflict of interest The authors declare no conflict of interests.

Ethical approval Not applicable.

References

Abramov, A.A., Eggleton, B.J., Rogers, J.A., Espindola, R.P., Hale, A., Windeler, R.S., Strasser, T.A.: Electrically tunable efficient broad-band fiber filter. IEEE Photonics Technol. Lett. **11**(4), 445–447 (1999)

Couny, F., Benabid, F., Light, P.S.: Subwatt threshold cw raman fiber-gas laser based on h2-filled hollow-core photonic crystal fiber. Phys. Rev. Lett. **99**(14), 143903 (2007)

Fan, X., Chen, H., Zheng, Y., Liu, Y., Chen, Q., Zhang, Y., Ma, M., Du, H., Li, S., Shum, P.P.: Ultrasensitive fiber-optic temperature sensor based on cascaded Sagnac interferometers with a nematic liquid crystal film. Opt. Laser Technol. **152**, 108169 (2022)

Ghosh, G., Endo, M., Iwasaki, T.: Temperature-dependent sellmeier coefficients and chromatic dispersions for some optical fiber glasses. J. Lightwave Technol. **12**(8), 1338–1342 (1994)

Han, T., Liu, Y., Wang, Z., Guo, J., Wu, Z., Wang, S., et al.: Unique characteristics of a selective-filling photonic crystal fiber sagnac interferometer and its application as high sensitivity sensor. Opt. Express **21**, 122–128 (2013)

Han, T., Liu, Y., Wang, Z., Guo, J., Wu, Z., Luo, M., et al.: Control and design of fiber birefringence characteristics based on selective filled hybrid photonic crystal fibers. Opt. Express **22**, 15002–15016 (2014)

He, J., Xu, B., Xu, X., et al.: Review of femtosecond-laser-inscribed fiber bragg gratings: fabrication technologies and sensing applications. Photonic Sens. **11**, 203–226 (2021)

Hirayama, N., Sano, Y.: Fiber bragg grating temperature sensor for practical use. ISA Trans. **39**(2), 169–173 (2000)

Hossain, M.S., Faisal, M.: Theoretical investigation of mid infrared temperature sensor based on sagnac interferometer using chloroform filled photonic crystal fiber. IEEE Sens. J. **21**(21), 24157–24165 (2021)

Ibrahim, J., Al Masri, M., Verrier, I., Kampfe, T., Veillas, C., Celle, F., Cioulachtjian, S., Lefevre, F., Jourlin, Y.: Surface plasmon resonance based temperature sensors in liquid environment. Sensors **19**(15), 3354 (2019)

Jiang, L., Zheng, Y., Hou, L., Zheng, K., Peng, J.: Surface plasmon induced polarization filter of the gold-coated photonic crystal fiber with a liquid core. Opt. Fiber Technol. **23**, 42–47 (2015)

Liu, Q., Li, S., Chen, H.: Enhanced sensitivity of temperature sensor by a PCF with a defect core based on sagnacnterferometer. Sens. Actuators B **254**, 636–641 (2018)

Liu, Y., Jing, X., Chen, H., Li, J., Guo, Y., Zhang, S., Li, H., Li, S.: Highly sensitive temperature sensor based on sagnac interferometer using photonic crystal fiber with circular layout. Sens. Actuators A **314**, 112236 (2020)

Liu, Z., Zhao, B., Zhang, Y., Zhang, Y., Sha, C., Yang, J., Yuan, L.: Optical fiber temperature sensor based on Fabry-Perot interferometer with photopolymer material. Sens. Actuators A **347**, 113894 (2022)

Ma, M., Chen, H., Li, S., Jing, X., Zhang, W., Liu, Y., Zhu, E.: Highly sensitive temperature sensor based on Sagnac interferometer with liquid crystal photonic crystal fibers. Optik **179**, 665–671 (2019)

Ma, L., Zhang, Y., Zhang, W., Li, Z., Gao, H., Ma, H., Yan, T.: High-performance all-fiber Mach-Zehnder interferometer based on D-shaped two-mode fiber coated with polydimethylsiloxane for temperature sensing. Opt. Fiber Technol. **71**, 102924 (2022)

Mahajan, S., Trivedi, V., Vora, P., Chhaniwal, V., Javidi, B., Anand, A.: Highly stable digital holographic microscope using sagnac interferometer. Opt. Lett. **40**, 3743–3746 (2015)

Qi, Y., Cong, B., Liu, Z., Gong, C., Li, F., Hu, T., Liu, Y.: All-fiber sensitivity-enhanced pressure sensor based on Sagnac and F-P interferometer. Optik **243**, 167359 (2021)

Shao, L., Luo, Y., Zhang, Z., Zou, X., Luo, B., Pan, W., Yan, L.: Sensitivity-enhanced temperature sensor with cascaded fiber optic sagnac interferometers based on Vernier-effect. Opt. Commun. **336**, 73–76 (2015)

Shi, J., Wang, Y., Xu, D., Zhang, H., Su, G., Duan, L., Yan, C., Yan, D., Fu, S., Yao, J.: Temperature sensor based on fiber ring laser withsagnac loop. IEEE Photonics Technol. Lett. **28**(7), 794–797 (2016)

Shi, M., Li, S., Chen, H.: A high-sensitivity temperature sensor based on Sagnac interferometer employing photonic crystal fiber fully filled with ethanol. Appl. Phys. B **124**, 94 (2018)

Wu, D., Zhao, Y., Hu, H.: Experimental research on FLM temperature sensor with an ethanol-filled photonic crystal fiber. Sens. Actuators A **209**, 62–67 (2014)

Yang, C., Zhang, H., Miao, Y., Liang, H., Zhao, X., Wang, Z., Liu, B.: Load-insensitive temperature sensor based on azobenzene-chloroform-solution-filled microstructured optical fiber. Opt. Lett. **38**, 5426–5429 (2013)

Zhang, B., Kahrizi, M.: High-temperature resistance fiber bragg grating temperature sensor fabrication. IEEE Sens. J. **7**(4), 586–591 (2007)

Zhang, S., Cao, Z., Xia, T., Yang, C., Liu, Z., Li, Z.: Lateral force sensing based on sagnac interferometry realized by a high-birefringence suspended-core fiber. J. Lightwave Technol. **40**(12), 3935–3941 (2022)

Zhao, C., Wang, Z., Zhang, S., Qi, L., Zhong, C., Zhang, Z., Jin, S., Guo, J., Wei, H.: Phenomenon in an alcohol not full-filled temperature sensor based on an optical fiber sagnac interferometer. Opt. Lett. **37**, 4789–4791 (2012)

Zhao, J., Zhao, Y., Bai, L., Zhang, Y.: Sagnac interferometer temperature sensor based on microstructured optical fiber filled with glycerin. Sens. Actuators A **314**, 112245 (2020)